Comparative study between three carbonaceous nanoblades and nanodarts for antimicrobial applications

M.S. Selim[1,2], A.M. Azzam[1,3], M.A. Shenashen[1,2,*] S.A. Higazy[2], B.B. Mostafa[3], S.A. El-Safty[1,4,*],

[1] National Institute for Materials Science (NIMS), 1-2-1 Sengen, Tsukubashi, Ibaraki-ken 305-0047, Japan.

[2] Petroleum Application Department, Egyptian Petroleum Research Institute (EPRI), Nasr City 11727, Cairo (Egypt).

[3] Department of Environmental Research, Theodor Bilharz Research Institute (TBRI), P.O. Box 30 -12411, Giza, Egypt.

[4] Faculty of Engineering and Advanced Manufacturing, University of Sunderland, St Peter's Campus, St Peter's Way, Sunderland SR6 0DD, UK.

E-mail: sherif.elsafty@nims.go.jp ; SHENASHEN.Mohameda@nims.go.jp;

Webpage: https://samurai.nims.go.jp/profiles/sherif_elsafty

Abstract:

This work reports a comparative study between the antimicrobial properties of graphene oxide (GO), reduced graphene oxide (RGO), and single-wall carbon nanotubes (SWCNTs). These nanoblades and nanodarts could have a mechano-bactericidal effect, piercing or slicing bacterial membranes. Nanoblades of GO nanosheets were successfully prepared using a modified Hummer's technique. RGO nanosheets were prepared by a hydrothermal reduction of GO at 180℃. These designed nanomaterials were well-characterized to elucidate the significance of the size, morphology, and elemental composition on the antibacterial activity mechanism. Gram-negative and gram-positive bacteria and fungi were used to investigate the nanomaterials' antimicrobial performance. The antibacterial efficacy of GO, RGO, and SWCNTs was assessed using the minimum inhibitory concentration (MIC), standard agar well diffusion, and transmission electron microscopy. The three nanomaterials were active against all tested microbial strains. These nanomaterials wrapped the bacterial cells completely and disrupted their morphology via microbial cell membrane degradation. They exhibited higher antibacterial efficiency toward gram-positive bacterial strains than gram-negative and fungi microorganisms, because their external cell wall structure and outer membrane proteins can reduce the permeability and protect against toxicants. Results showed that the antimicrobial activity of these nanomaterials was in the order RGO > GO > SWCNTs. RGO had the lowest MIC values (0.062, 0.125, and 0.25 mg/mL against *B. subtilis, S. aureus,* and *E. coli*, respectively) as well as minimum fungal concentrations (0.5 mg/mL for both *A. fumigatus* and *C. albicans*). Its cell viability values toward different microbial strains reached a complete inhibition after only 12 hr. Microorganisms perching on RGO nanoblades suffered from significant membrane damage, resulting in cell lysis and death. Our work gives an insight into the design of effective graphene-based antimicrobial materials for water treatment and remediation.

Keywords: *Antimicrobial properties; nanoblades; mechano-bactericidal effect; RGO nanosheets; gram-positive bacteria; cell viability.*

1. Introduction

Nanomaterial science advancements have led to significant technological advancements in various applications such as medical, manufacturing, energy production, pollution control, and environmental cleanup (Selim et al., 2017). Pollution of water resources, including river pollution and drinking water contamination caused by industrial wastes, animal farms, and agricultural activities. These activities can release unreacted organic dyes and heavy residual materials which are a worldwide environmental threat (Liu et al., 2018; Kumwimba et al., 2018). These organic chemicals in wastewater stimulate the synthesis of hazardous metabolites, increase microbial development in rivers, and cause water-borne disorders because of the high microbial density (Orou et al., 2018). Recent research on "Clean Rivers" to alleviate the problem of water pollution has been prompted by these global threats (Gonzales-Gustavson et al., 2017). Degradation of organic pollutants and microbial growth inhibition by chemical-physical procedures and chemical oxidation processes are examples of modern strategies for minimizing water pollution (Varjani and Upasani et al., 2017). However, in these procedures, the formation of secondary sludge is a big problem (Shabanzade et al., 2018). Furthermore, the capacity of microbial organisms for evolving biological resistance negates the effects of antibacterial materials (Fatthallah et al., 2021). As a result, developing advanced antibacterial and antibiofilm nanomaterials is required for water treatment and sustainable development (Askar et al., 2021).

Bacterium contact with nanoscale materials in an aqueous media exhibit a significant antibacterial impact (Mokammel et al., 2022; Li et al., 2022). Mechano-bactericidal nanostructures have instant advantages over chemical-based antibacterial therapies, because of these nanostructures' physical interactions with bacteria and they don't release antibacterial substances (Wang et al., 2016). Carbonaceous-based antimicrobial surfaces, particularly graphene materials and carbon nanotubes (CNTs) are currently one of the hottest study areas (Samak et al., 2020). Sharp nanostructured materials with high-surface area can swiftly remove adherent microbial strains after only minutes of contact. Graphene oxide (GO), reduced GO (RGO), and single-walled

carbon nanotubes (SWCNTs) are smart antimicrobial agents because their morphostructural properties can be controlled to limit their biotoxicity (Lin et al., 2018; Selim et al., 2018). Direct contact with SWCNTs can puncture and destroy the cell wall of *E. coli*, implying that SWCNTs could be used as antibacterial materials under the mechano-bactericidal mode (Al-Jumaili et al., 2017). Because of the agglomerations of multi-walled CNTs (MWCNTs), they had lower bactericidal efficiency than SWCNTs (Teixeira-Santos et al., 2021; Yuan et al., 2019). SWCNTs were found to have greater antibacterial activity than MWCNTs caused by the high aspect ratio geometry of SWCNTs. Longer nanotubes have better antibacterial action at the same weight concentrations (Safdar et al., 2022). The greater specific surface area allows more interactions with cell membranes and results in more membrane piercing (Yuan et al., 2019). Rigid and thin SWCNTs caused greater penetrating, dart-like damage to gut bacteria membranes than MWCNTs (Chen et al., 2013).

As two-dimensional materials, graphene-derivatives (including GO and RGO nanosheets) have a high aspect ratio and exhibit high antibacterial activity (Xia et al., 2019). The sharp graphene edges cause mechano-bactericidal performance upon physical interaction with bacteria (Linklater et al., 2021). They are biocompatible materials with low toxicity to human and mammalian living cells, making them environmentally friendly. RGO offers various advantages, including superior hydrophobicity, high-surface area, high yield, biocompatibility with human and mammalian live cells, excellent processability, cost savings, and antibacterial performance (Thebo et al., 2018; Naskar et al., 2018). Individually dispersed SWCNTs were more hazardous to bacteria than aggregated SWCNTs (Liu et al., 2009). They acted as many moving "nanodarts" in solution, constantly attacking bacterial cells and causing bacterial cell integrity breakdown, which led to cell death (Parwez, and Budihal, 2019). GO, RGO, and CNTs were heavily regarded as potent antibacterial and antimicrobial active materials. The mechanism happens when bacterial cell integrity is disrupted as a result of direct contact with the selected carbonaceous material, which can

kill the cell (Xin et al., 2019; Azizi-Lalabadi et al., 2020). However, the intricate antimicrobial activity mechanisms of GO, RGO, and SWCNTs are still a mystery.

For the first time, this work investigated and compared the antibacterial efficacy between GO and RGO nanoblades and SWCNT nanodarts. These carbonaceous nanomaterials exhibited a diverse range of nanoscale sizes, morphologies, elemental composition, and surface exposure topologies. A modified Hummers' approach was used to create GO sheets. RGO was prepared by a hydrothermal reduction of GO at 180℃. The antibacterial efficiency of GO, RGO, and SWCNT was studied using gram-positive bacteria (*Bacillus subtilis and Staphylococcus aureus)*, gram-negative bacteria (*Pseudomonas aeruginosa and Escherichia coli*), and fungi (*Aspergillus fumigatus and Candida albicans*). The cell viability, minimum inhibitor concentration (MIC), and transmission electron microscopy (TEM) were used to investigate the nanomaterials' bacterial resistance and morphology wrapping and disruption in the cellular membrane. The developed RGO nanoblades exhibited higher antibacterial activity than GO and CNTs against various microbial strains. The antibacterial mechanism of the produced blade-like and dart-like nanomaterials was discussed extensively. This work prompts a modern research gateway for facilitating the next generation of antibacterial carbonaceous nanostructured materials for the sustainable environment.

2. Materials & Methods

2.1. Materials

Sigma-Aldrich Company in the United States provided graphite flakes (< 20 μm, synthetic) and sodium nitrate (99%). NaOH (98%) and $KMnO_4$ (99%) were delivered from Aladdin Industrial co., Shanghai, China. H_2O_2 (35%), H_2SO_4 (95%), and ethanol (AR) were provided by Acros Company, Belgium. SWCNTs with a diameter distribution of 1.5 nm, length of 500-1000 nm, 99% purity were purchased from Xuzhou Jie-Chuang New Material Technology Co., Ltd. China. The used solvents were of high purity and used exactly without further purification. All the employed materials were

analytical reagents used as obtained. All the used microorganisms were obtained from the Environmental Research Department, Theodor Bilharz Research Institute, Egypt (TBRI) and growth media were obtained from Hi-Media, Mumbai, India.

2.2. Synthesis methods

2.2.1. Preparing GO nanosheets

The modified Hummer's process generates GO nanosheets by oxidizing graphite powder (Rajapaksha et al., 2019; Liu et al., 2018) as follows: 1.5 g graphite flakes and 1.5 g $NaNO_3$ were dissolved into 72 mL H_2SO_4 under constant stirring. $KMnO_4$ (9 g) was gently mixed and stirred for 1 hr (35℃) to prevent the suspension temperature from reaching 20℃. After dilution with 120 mL distilled water and slow addition of 15 mL H_2O_2, the temperature was raised to 90℃. A suspension was created and filtered with deionized H_2O until the pH reached 7. The obtained yellow-brown suspension was ultrasonically exfoliated and centrifuged to yield GO nanosheets and eliminate the un-exfoliated precipitation.

2.2.2. Preparing RGO nanosheets

A specific amount of the produced GO sheets was ultrasonically treated in deionized H_2O for 30 minutes. This dispersed mixture was put into an autoclave lined with Teflon and subjected to a hydrothermal reduction process for 8 hr at 180℃ (Scheme 1). The reduction product was naturally cooled before being centrifuged to yield RGO sheets. The product was purified by washing it with an ethanol/distilled H_2O mixture and then freezing it for 1 day at -45℃ to remove the adsorbed solutions and yield homogeneous RGO sheets (Samak et al., 2022).

2.3. Characterization techniques

FTIR analysis of the developed nanostructures was performed by Nicolet™ iS™10 (Thermo Fisher Scientific, USA) and KBr pellets. X-ray diffraction (XRD) was analyzed by the X'Pert PRO diffraction device (PANalytical, Netherlands) to investigate the products' purity and crystallinity. CuKα radiation was used to get the XRD pattern at 2θ of 5°–80°. A TEM instrument model JEM

2100 LaB6 (JEOL, Japan) was used to examine TEM images of the developed nanomaterials at 200 kV. FESEM (JSM530, JEOL, Japan) was employed at 30 kV to examine the morphology and size of the nanomaterials. Two droplets of the nanomaterials' solutions were put over a glassy sample, dried, and subjected to gold-spatter coating for preventing the electron beam's charging.

2.4. Carbonaceous materials' antimicrobial activity

The microbial resistance of GO, RGO, and SWCNTs was investigated by standard agar well diffusion procedure against different bacterial strains, including *Staphylococcus aureus* and *Bacillus subtilis* (Gram-positive), *Escherichia coli* and *Pseudomonas aeruginosa* (Gram-negative) bacteria and *Aspergillus fumigatus* and *Candida albicans* (fungi). These strains represent essential pathogens and are widely spread in water sources (Selim et al., 2020a). They are highly adaptable to different environmental conditions and are extensively applied to assess the biological behavior of nanomaterials (Hao et al., 2020; Selim et al., 2020b).

Fresh pure cultures of these microbes were subcultured in Müller-Hinton and Sabouraud Dextrose broth. Nutritional agar for bacteria and Sabouraud Dextrose agar (SDA) plates were kept standing for 15 min after pouring. The carbonaceous materials' antimicrobial activities were then tested using 6.0 mm holes in plates. 100 µL water suspension (10.0 mg/mL) of the carbonaceous materials was put into each well of all plates using a micropipette. The varying amounts of inhibition zone were evaluated during overnight incubation at 37℃ for bacterial organisms for 2 days, while for fungi the evaluation was performed at 28℃. For every concentration and organism, duplicate plates were utilized (Ranjani et al., 2021). *The B. subtilis, S. aureus, P. aeruginosa*, and *E. coli* strains were also cultivated overnight on MHA plates at 37℃ before use. The MIC was evaluated in nutritional broth Hi-Media (Mumbai, India) using successive two-fold dilutions of the selected materials in concentrations ranging from 100-5000 mg/mL, initial bacterial inoculums of 0.5 McFarland turbidity, and incubation for 24 hr at 37℃. MIC represents the lowest antimicrobial concentration which prevents 99% of bacteria from growing. The MIC value for each tested microorganism was determined in triplicate to ensure accuracy (Yayehrad et al., 2022). By plating

loopful of *A. fumigatus* and *C. albicans* culture onto Sabouraud Dextrose Agar (SDA) plates and incubating under aseptic conditions for 72 hr at 28℃, the MFC of the CNTs, GO, and RGO were determined. The MFC is the lowest concentration of CNTs, GO, and RGO that demonstrated no observable development on solid media (Asl et al., 2021).

Viable microbial counts (VMCs) assay was evaluated for each microbial species at different times after being treated with 10 mg/mL of RGO nanosheets, then the count of surviving microbial cells was determined by plate count technique. Using Eq.1, the reduction percentage of total VMCs was calculated after treating cells with RGO:

$$\text{VBCs Reduction \%} = \frac{\text{Viable count at time 0} - \text{Viable count at time x}}{\text{Viable count at time 0}} \text{ X } 100 \qquad (1)$$

where time 0 is the time before adding RGO nanosheets and time x is the contact time between microbial cells and RGO nanosheets.

Additionally, Elbasuney et al. (Elbasuney et al., 2021) reported a qualitative examination of the suppression of biofilm formation. In the absence and presence of carbonaceous nanoparticles, the inhibition of biofilm investigation was conducted using a tube wall method (Elbasuney et al., 2022). The antibiofilm activity of these nanomaterials (at 10.0 mg/mL) was tested against the selected microorganisms (*S. aureus*, *E. coli*, and *C. albicans*) and compared to the control sample. In brief, nutrient broth medium (5 mL) was utilized in the whole tubes, and the examined microbes were inoculated and adjusted to 1–3.5×10^8 CFU/mL using 0.5 McFarland. The cells were then cultured for 24 hr at 37℃. The media from the control sample and treated tubes were taken out, and then Phosphate Buffered Saline (PBS) with PH=7.0 was mixed and stored. Then, the adhering microbial cells were treated for 20 min with sodium acetate (5 mL, 3.5%). The deionized water was used to clean them. Then, 20 mL Crystal Violet (CV) with 0.15% concentration was employed to dye biofilms followed by rinsing with DW for removing any excess CV. For separating the stained microbial films for the semiquantitative antibacterial evaluation, 5 mL of absolute ethanol was applied. The O.D. (for stained biofilms of bacteria and fungi) was measured at 570 nm with a UV-

Vis spectrophotometer (El-Batal et al., 2019). Using Eq.2, the microbial biofilm inhibition's proportion was evaluated (Ansari et al., 2014):

The percentage of biofilm inhibition = $((O.D._{control} - O.D._{treated})/O.D._{control}) \times 100$ (2)

2.5. The treated bacteria and fungi strains' morphological investigation

A TEM EM 208S instrument (Philips, Netherlands) instrument was used to examine bacterial and fungal cells in both treated and untreated samples. After being fixed in 1% glutaraldehyde and washed in 0.1 M buffer, the specimens were subjected to post-fixing into Osmium tetraoxide (1 wt.%) and washed in 0.1 M buffer. The specimens were infiltrated and implanted in epoxy resin after being dehydrated in acetone. Lastly, the TEM meshes were dried and captured via the JEOL 1010 instrument (Japan) to investigate morphological changes caused by the selected carbonaceous materials' biocidal effect (Karmakar et al., 2022).

3. Results & Discussion

3.1. GO, RGO, and CNTs morphologies and sizes

The OH stretch modes on the surface of the GO sheets produced FTIR peaks at 3740 cm^{-1} (**Fig. 1**A (a)). The symmetric and non-symmetric stretching modes of CH_2 units were observed at 2890 and 2956 cm^{-1}. Also, the peaks observed at 1739 and 1339 cm^{-1} were those of the stretching C=O carboxylic as well as C-OH alcoholic vibrations. The non-oxidized graphene C=C peak was detected at 1628 cm^{-1}. The peak at 665 cm^{-1} was owed to epoxide units on the GO sheet's edges. The absence and reduction in the hydroxyl and carbonyl groups in the spectrum (**Fig. 1**A (b)) indicated that GO was reduced to RGO using the hydrothermal technique. This assured the removal or decrease of the surface C-OH and C=O throughout the reduction procedure. The C=O binding changes were also recorded in the region at 1717 cm^{-1} in the FTIR peak of SWCNTs (**Fig. 1**A(c)). Furthermore, C-C binding vibrations in CNTs were recorded at 1538 cm^{-1}. **Fig. 2** depicted the XRD results of the used materials. XRD analysis of the prepared GO sheets (**Fig. 1**B(a)) revealed that the main peak observed at $2\theta = 10.4°$ was owed to (001) orientation which exhibited a d-spacing of

0.95 nm. This was greater than the 0.335 nm d-spacing of exfoliated natural graphite; which could increase the interlayer distance between the functionalized oxygen on the surface. XRD pattern of RGO was reflected in **Fig. 1**B(b) at 2θ = 23.28° which owed to (002) crystalline orientation. Those results assured the preparation of nano-RGO sheets in dispersed form without aggregations. Furthermore, CNTs' XRD pattern (**Fig. 1**B(c)) shows two typical peaks at 2θ = 25.3° as well as 42.8°. These peaks correspond to SWCNTs' (002) and (100) crystal orientations (JCPDS No. 01-075-1621). FETEM device captured the products' morphology (**Fig. 2**). **Fig. 2** (A and B) of the nano-GO showed wrinkled nanosheets including folded regions at the edges. In addition, the nanosheet structure of nano-RGO with 2 nm sheet thickness was confirmed (**Fig. 2** (C and D)). Also, FETEM analysis could study the SWCNTs' shape and size. The observed SWCNTs observed was homogeneous and had a diameter of nearly 1 nm, as seen in the HRTEM image (**Fig. 2** (E and F)). The results also showed that the tested material was pure, i.e. free of metallic impurities and amorphous carbon deposits. **Fig. 3** depicted the morphology and nanostructures of the materials produced using FESEM images. FESEM captures in **Fig. 3** (A and B) depicted the designed GO shape and structure. The FESEM of RGO revealed layered nanosheets with wrinkled edge structures (**Fig. 3** (C and D)). Meanwhile, FESEM images of SWCNTs showed nanotube lengths ranging from 100 nm to 500 nm with uniform diameters of 1.5 nm, **Fig. 3** (E and F)). The images of the SWCNT showed a smooth and uniform surface.

3.2. Antimicrobial activity of carbonaceous nanomaterials

The different inhibition zones of three tested carbonaceous nanomaterials (10.0 mg/mL) and positive control antibiotics against different microbes were illustrated in **Fig. 4**. The highest recorded inhibition zone was presented by RGO. Also, the selected carbonaceous materials exhibited high antibacterial performance toward gram-positive bacteria than gram-negative strains and fungi. Moreover, *B. subtilis* and *S. aureus* (G-positive bacteria) exhibited the highest inhibition zones, 20.0±2.0 and 19.0±1.5 mm with RGO, respectively. However, *E. coli, A. fumigatus, C.*

albicans, and *P. aeruginosa* were recorded at 17.5±1.0, 14.0±1.0, 12.7±1.0, and 12.5±1.0 with RGO, respectively. These results are in agreement with those reported by Naseer et al. (Naseer et al., 2020). They stated that Fe_2O_3/RGO nanocomposite could significantly inhibit the growth of *S. aureus,* vancomycin-resistant *S. aureus*, and ciprofloxacin-resistant *S. aureus* bacteria in the range of 10–5000 μg/mL

Fig. 5 showed the MIC of CNTs, GO, and RGO that were detected for different bacterial and fungal species. The recorded MIC values of RGO were the lowest ones recorded at 0.062, 0.125, 0.25, 0.5, 0.5, and 1.0 mg/mL against *B. subtilis, S. aureus, E. coli*, *A. fumigatus, C. albicans,* and *P. aeruginosa*, respectively. However, the CNTs and GO recorded higher concentrations. Thus, RGO is a promising antimicrobial agent that can be developed and utilized in wastewater purification for the inactivation of waterborne microbial species that causes harmful diseases for human and contaminates our hydrosphere. Kellici and his coworkers (Kellici et al., 2014) recorded MIC 125 μg mL^{-1} for RGO against the gram-negative bacterium *E. coli*.

As shown in **Fig. 6**, the VMCs reduction percent of *B. subtilis* and *S. aureus* bacteria that treated with RGO at 9 and 12 hr of contact time reached 100% inhibition, respectively, whereas, *E. coli* and *A. fumigatus* was treated for 18 hr. However, complete inactivation occurred for *P. aeruginosa* and *C. albicans* after 24 hr of contact time.

3.3. Antibiofilm performance assessments

Exo-polysaccharide synthesis promotes the biofilm formation by pathogenic bacteria and fungi (Singh et al., 2021). The antibiofilm behaviour of carbonaceous materials against unicellular microbes was defined using a tube design. On the other hand, a substantial negative influence was detected in the tubes containing microbial cells and the three carbonaceous nanomaterials, as the cells didn't create biofilm layers and the ring building was stopped. Furthermore, the adhering cells' color was only a faint blue tint formed once ethyl alcohol was added (Kasim et al., 2016). **Fig. 7** shows the percentage of biofilm inhibition for *S. aureus, E. coli,* and *C. albicans* after the addition

of 10.0 mg/mL of three carbonaceous nanomaterials. RGO demonstrated the highest percentage inhibition of 55%, 45%, and 40% against *S. aureus, E. coli, and C. albicans,* respectively. GO was also slightly more active than CNTs. Notably, RGO inactivated the formation and cohesion strength of the biofilm and provided high antibacterial performance (Zhang et al., 2020). The difference in the hindrance % could be attributable to the antimicrobial agent's high capacity to connect to the surface due to RGO's structure. The attack style of these groups also has an impact on their interactions and affiliation with biofilm-producing bacteria (El-Batal et al., 2020).

The antimicrobial efficiency of graphene materials is usually dependent on the physicochemical interactions between the sheets and pathogenic microbes (Omran et al., 2022). RGO nanosheets can pierce the bacterial cellular membrane with their sharp edges, resulting in pore formation, changes in bacterial osmotic pressure, and cell death (Pham et al., 2015). Choudhary et al. (2017) reported that the presence of carboxyl, hydroxyl, amine, and phosphate groups of the intracellular protein provided enormous binding sites for conjugation with RGO through covalent, hydrophobic, and π–π stacking interactions with sp^2 bonded carbon atom. The RGO thus interacts with cell membrane proteins through hydrogen bonding, π–π stacking, and electrostatic interactions by making contact with the microorganism. Membrane stress is initiated when RGO pierces the bacterial cell membrane with blade-like edges, causing leakage of intracellular constituents, and cell death. RGO nanosheets have a relatively high surface area due to their sharp edges, making them attractive as direct-contact bactericidal agents (Mann et al., 2021). The cellular membranes trapped the graphene tail end as a result of van der Waals attraction forces and hydrophobic interactions. The nanosheet can pierce the lipid bilayer membrane. RGO destabilizes cell membrane by inducing mechanical stress and also by triggering reactive oxygen species (ROS) generation. Sengupta et al. (2019) reported the antibacterial activity of GO and RGO on gram-positive *Staphylococcus aureus* and gram-negative *Pseudomonas aeruginosa* bacteria. They concluded that GO destructed bacteria by cell membrane damage through chemical reaction whereas, RGO sheets induced mechanical stress and pierced the cell membrane. Gusev and his coworkers (Gusev et al., 2019) performed

microscopic and zeta potential studies of RGO-bacteria interactions. They indicated the electrostatic nature of the interaction of RGO and bacteria, which could be mediated via hydrogen bonding between the cell walls of *E. coli* and RGO functionalities. Because of the presence of these oxygen functional groups in both RGO and cell membranes, the aggregation of RGO sheets and bacteria mediated via hydrogen bonding was expected. Their optical photographs studies showed that the bacteria were localized on the RGO but not on a bare substrate, suggesting strong interaction between bacteria and RGO, which was likely mediated by hydrogen bonding.

3.4. Bacterial morphological studies

The putative antibacterial mechanism against *S. aureus* and *E. coli* was investigated using TEM imaging analysis. In the absence of RGO nanomaterial, TEM inspection of the control bacteria revealed that they were growing normally with typical budding surfaces and solid cell membranes, as shown in **Fig. 8** (A and C). Both bacterial species showed significant morphological abnormalities after RGO treatment (**Fig. 8** (B and D)), including entire cell membrane lysis, as demonstrated by bacterial cell deformation. Furthermore, the RGO produced full lysis of the bacterial cells as well as cell deformation, resulting in a decrease in the total number of viable cells. Effective mechanisms, including the dispersion of ROS, may be created by the active groups of the RGO surface (El-Batal et al., 2018). The RGO nanomaterial is thought to start its activity by wrapping and attaching to the microbial cells' outer surface, inducing membrane breakdown and altering the transport potential (Maksoud et al. 2020). All internal structures, including plasmid, DNA, and other important organelles, are divided when microbial cells' interior components are reacted with RGO. Finally, cellular toxicity occurs as a result of oxidative stress induced by the ROS's production which causes cellular and genotoxicity as a result of interactions among negatively charged essential organelles (Ashour t al., 2018).

- The RGO action mechanism combines the synergetic effects of the nanosheets' blade-like edges.
- The RGO nanosheets' edges function as nanoblades, putting bacterium-mechanical stress over microbial cell membranes and inflicting physical damage. The disintegration of the cell wall causes

RNA spills. Carbon-free radicals develop on the microbial surface, causing cell structural damage and creating oxidative stress. Thus, the cell membrane broke and shattered, triggering lysis, which forced the cellular components out of the cell.

- The the antibacterial characteristics of SWCNTs are caused by the high the aspect ratio and small diameter. Graphene materials with larger degrees of sharp edge-asperities follow the same pattern. The antibacterial activity of graphene materials in both colloids and nanotopography is increased by enhancing the aspect ratio by developing sharper or thinner nanosheets.

The presence of many wrinkles on the RGO surface can reduce surface energy and improve the stability of the aqueous medium (Boukherroub, 2016). The high RGO edges' oxygen content can minimize the repulsion between hydrophilic edge atoms and hydrophobic lipid tails, resulting in a trans-membrane nanostructure. RGO alters the osmotic pressure of microbial cells and causes cells to enlarge and die by acting as pores in the cell membrane (Pham et al., 2015).

- RGO nanosheets' lateral edge may increase the permeability of cell membrane, leading to the tearing cell wall (Linklater et al., 2018). The cell wall break disrupts cellular signaling and electron transport through the cell membrane. The high oxidative stress on microbial cells leads to more disturbance in the bioactivities of cells through inhibition of growth and lysis of internal cellular components or death. The produced ROS can injure cells while also functioning as an antibacterial agent.

- RGO nanosheets exhibited ultra-higher conductivity than nano-GO, which is electrically insulating (Devi and Kumar, 2018). Thus, RGO with higher conductivity can exhibit better glutathione oxidation capabilities than the lower conductive GO sheets. RGO was found to have better antibacterial action than GO against both bacterial types in a fascinating investigation (Mohamed et al., 2020). Also, RGO increases the conductivity through cell membrane lipid layers, interfering with electron transport from the bacterial inner milieu to the exterior environment. RGO antibacterial action is based on electron transfer rather than ROS (Li et al., 2015).

Another study found that RGO suppressed *E. coli* multiplication while showing no cytotoxicity

(Zheng et al., 2017; Lu et al., 2016). RGO nanosheets exhibited high surface area and strength. As a result, RGO generations partially restore graphene properties. In a fascinating investigation, RGO outperformed GO in bactericidal effect against *S. aureus* and *E. coli.* Another study found that RGO suppressed *E. coli* multiplication while GO had no cytotoxicity. In addition, the wrinkled edges of RGO nanosheets interact with aqueous media, stabilizing the RGO combination's structure and resulting in long-lasting antibacterial action. The RGO exhibited a large dispersion capability in an aqueous medium due to their potent microbicidal effect and the wide surface that interact with microbes.

Herein, the TEM results showed cellular alteration and damage appeared in the form of cellular fragmentation, wrinkled abnormalities, viability, and integrity loss. These alterations are the consequences of oxidative stress caused upon contact of blade-like edges of RGO and the bacterial cell walls. Generally, oxidative stress is the major symptom of RGO toxicity. The produced ROS by RGO nanosheets and their sharp edges lead to cellular lysis upon contact with bacterial cell walls to end with microbial cytotoxicity and death (Shulga and Shulga, 2019). TEM, MIC, and cell viability are the major tools employed to express the RGO antibacterial mode of action. Selim and coworkers (Selim et al., 2020a) demonstrated the antimicrobial efficiency of the blade-like GO/Cu_2O which was elucidated by electron microscopy. They concluded that the complete microbial cell is subjected to oxidative stress of high levels of ROS leading to DNA damage and cellular degradation ending in microbial growth inhibition, cytotoxicity, or death. Samak et al. (2022) used SEM analysis to study the antibacterial mechanism of RGO/metal oxide nanocomposite and concluded that the lateral edges of the RGO nanosheets and electrostatic interactions of metal oxide nanoparticles may increase the permeability of the cellular membrane. The microbial cell is then exposed to oxidative stress, which causes cellular disintegration leading to microbial growth suppression, cytotoxicity, or death (Pieper et al., 2016). Mohamed et al. (2020) reported that graphene materials hold a high affinity to the membrane proteoglycans where they accumulate leading to membrane damage. After internalization, they can interact with bacteria interrupting the replicative stage. RGO interacts with bacteria through hydrogen

bonding, π-π stacking, and electrostatic adsorption due to the presence of oxygen- and nitrogen-containing groups in addition to the π-conjugated structure (He et al., 2010). Graphene materials' permeation into the microorganism alters the DNA structures and properties leading to the inactivation or death of the microorganism (Hadidi and Mohebbi, 2022).

4. Conclusions:

To combat the negative effects of microbial strains, the current study introduces three carbonaceous materials with high antibacterial properties for water resource control and remediation. Mechano-bactericidal nanostructures, as antibacterial surfaces that do not emit chemicals, provide opportunities for the development of long-lasting antimicrobial materials. For the first time, this study compared the antibacterial and antibiofilm properties of three different carbon-based materials (GO, RGO, and CNTs). A modified Hummer's method was used to synthesize ~2 nm sheet thickness of nano-GO. RGO sheet morphology was produced using a hydrothermal method. Carbonaceous-mediated toxicity is determined by physiological properties such as size, concentration, and surface features. Discussing the carbon-based antibacterial mechanism against various bacterial organisms was unavoidable. RGO nanosheets exhibited a uniform distribution and outperformed GO and SWCNTs in antibacterial performance. RGO demonstrated the highest antibacterial activity toward various microbes with 55 %, 45 %, and 40 % antibiofilm inhibition percentages for the tested unicellular microbes *S. aureus (*gram-positive bacterial strains), *E. coli* (gram-negative organisms), and *C. albicans* (fungi), respectively. The RGO sheets' antimicrobial performance was discussed through microbial physical wrapping as well as covalent and π-π interactions with the microbial cellular membranes. The RGO nanobaldes with high surface area induce oxidative stress, cellular destruction and lysis, physical wrapping, mechanical stress, and cytotoxicity. These fascinating antimicrobial carbon-based materials can introduce an advanced and controlled model for water treatment and antibiotic resistance. The current study encourages the development of futuristic RGO-derived nanocomposites for

environmental sustainability. Understanding bacterial interactions with mechano-bactericidal nanostructures will aid in defining optimal geometry and dimensions in the future. It presents a simple model that may inspire further experimental and theoretical research on carbonaceous-based materials as antibacterial active agents.

Conflicts of interest

The authors declare no conflicts of interest.

Acknowledgement

This work was supported by the Center for Functional Materials, National Institute for Materials Science (NIMS in Japan), Egyptian Petroleum Research Institute (EPRI in Egypt), and Nano-Environmental Uint (NEU), Theodor Bilharz Research Institute (TBRI in Egypt).

References:

Al-Jumaili, A., Alancherry, S., Bazaka, K., Jacob, M.V., 2017. Review on the antimicrobial properties of carbon nanostructures. Materials 10, 1066.

Ansari, M.A., Khan, H.M., Khan, A.A., Cameotra, S.S., Pal, R., 2014. Antibiofilm efficacy of silver nanoparticles against biofilm of extended spectrum β-lactamase isolates of *Escherichia coli* and *Klebsiella pneumonia*. Appl. Nanosci. 4, 859–868.

Ashour, A.H., El-Batal, A.I., Maksoud, M.I.A.A., ElSayyad, G.S., Labib, S., Abdeltwab, E., et al., 2018. Antimicrobial activity of metal-substituted cobalt ferrite nanoparticles synthesized by sol–gel technique. Particuology 40, 141–151.

Askar, A.A., Selim, M.S., El-Safty, S.A., Hashem, A.I., Selim, M.M., Shenashen, M.A., 2021. Antimicrobial and immunomodulatory potential of nanoscale hierarchical one-dimensional zinc oxide and silicon carbide materials. Mater. Chem. Phys. 263, 124376.

Asl, N.M., Ahari, H., Moghanjoghi, A.A.M., Saeed, P., 2021. Assessment of nanochitosan

packaging containing silver NPs on improving the shelf life of caviar (*Acipenser persicus*) and evaluation of nanoparticles migration. Food Measure 15, 5078–5086.

Azizi-Lalabadi, M., Hashemi, H., Feng, J., Jafari, S.M., 2020. Carbon nanomaterials against pathogens; the antimicrobial activity of carbon nanotubes, graphene/graphene oxide, fullerenes, and their nanocomposites. Adv. Colloid Interface Sci. 284, 102250.

Boukherroub, S.S.R., 2016. Antibacterial activity of graphene-based materials. J. Mater. Chem. B. 4, 6892–6912.

Chen, H., Wang, B., Gao, D., Guan, M., Zheng, L., Ouyang, H., et al., 2013. Broad-spectrum antibacterial activity of carbon nanotubes to human gut bacteria. Small 9(16), 2735-2746.

Choudhary, P., Parandhaman, T., Ramalingam, B., Duraipandy, N., Kiran, M.S., Das, S.K., 2017. Fabrication of non-toxic reduced graphene oxide protein nanoframework as sustained antimicrobial coating for biomedical application. ACS Appl. Mater. Interfaces 9 (44) 38255–38269.

Devi, M., Kumar, A., 2018. Structural, thermal and dielectric properties of in-situ reduced graphene oxide − polypyrrole nanotubes nanocomposites. Mater. Res. Bullet. 97, 207-214.

Elbasuney, S., El-Sayyad, G.S., Tantawy, H., Hashem, A.H., 2021. Promising antimicrobial and antibiofilm activities of reduced graphene oxide-metal oxide (RGO-NiO, RGO-AgO, and RGO-ZnO) nanocomposites. RSC Adv. 11, 25961–25975.

Elbasuney, S., Yehia, M., Ismael, S., Al-Hazmi, N.E., El-Sayyad, G.S., Tantawy, H., 2022. Potential impact of reduced graphene oxide incorporated metal oxide nanocomposites as antimicrobial, and antibiofilm agents against pathogenic microbes: Bacterial protein leakage reaction mechanism, J Clust. Sci. https://doi.org/10.1007/s10876-022-02255-0

El-Batal, A.I., El-Sayyad, G.S., Al-Hazmi, N.E., Gobara, M., 2019. Antibiofilm and antimicrobial activities of silver boron nanoparticles synthesized by PVP polymer and gamma rays against urinary tract pathogens. J. Cluster Sci. 30, 947–964.

El-Batal, A.I., Mosallam, F.M., El-Sayyad, G.S., 2018. Synthesis of metallic silver nanoparticles by fluconazole drug and gamma rays to inhibit the growth of multidrug-resistant microbes. J. Cluster

Sci. 29, 1003–1015.

El-Batal, A.I., Nada, H.G., El-Behery, R.R., Gobara, M., El-Sayyad, G.S., 2020. Nystatin-mediated bismuth oxide nano-drug synthesis using gamma rays for increasing teh antimicrobial and antibiofilm activities against some pathogenic bacteria and *Candida species*. RSC Adv. 10, 9274–9289.

Fatthallah, N.A., Selim, M.S., El Safty, S.A., Selim, M.M., Shenashen, M.A., 2021. Engineering nanoscale hierarchical morphologies and geometrical shapes for microbial inactivation in aqueous solution. Mater. Sci. Engin. C 122, 111844.

Gonzales-Gustavson, E., Cárdenas-Youngs, Y., Calvo, M., Marques da Silva, M.F., Hundesa, A., Amorós, I., et al., 2017. Characterization of the efficiency and uncertainty of skimmed milk flocculation for the simultaneous concentration and quantification of water-borne viruses, bacteria and protozoa, J. Microbiol. Methods 134, 46-53.

Gusev, A., Zakharova, O., Muratov, D.S., Vorobeva, N.S., Sarker, M., Rybkin, I., et al., 2019. Medium-dependent antibacterial properties and bacterial filtration ability of reduced graphene oxide. Nanomaterials, 9, 1454.

Hadidi, N., Mohebbi, M., 2022. Anti-infective and toxicity properties of carbon based materials: Graphene and functionalized carbon nanotubes. Microorganisms 10 (12), 2439.

Hao, X., Chen, S., Qin, D., Zhang, M., Li, W., Fan, J., et al., 2020. Antifouling and antibacterial behaviors of capsaicin-based pH responsive smart coatings in marine environments. Mater. Sci. Engin. C 108, 110361.

He, S., Song, B., Li, D., Zhu, C., Qi, W., Wen, Y., et al., 2010. A graphene nanoprobe for rapid, sensitive, and multicolor fluorescent DNA analysis. Adv. Funct. Mater. 20, 453–459.

Karmakar, A., Hazra, S., Pombeiro, A.J.L., 2022. Urea and thiourea based coordination polymers and metal-organic frameworks: Synthesis, structure and applications. Coord. Chem. Rev. 453, 214314.

Kasim, W.A., Gaafar, R.M., Abou-Ali, R.M., Omar, M.N., Hewait, H.M., 2016. Effect of biofilm

forming plant growth promoting *rhizobacteria* on salinity tolerance in barley. Ann. Agricultural Sci. 61(2), 217-227.

Kellici, S., Acord, J., Ball, J., Reehal, H.S., Morgan, D., Saha, B., 2014. A single rapid route for the synthesis of reduced graphene oxide with antibacterial activities. RSC Adv. 4, 14858-14861.

Kumwimba, M.N., Meng, F., Iseyemi, O., Moore, M.T., Zhu, B., Tao, W., et al., 2018. Removal of non-point source pollutants from domestic sewage and agricultural runoff by vegetated drainage ditches (VDDs): Design, mechanism, management strategies, and future directions. Sci. Total Environ. 639, 742-759.

Li, B., Luo, Y., Zheng, Y., Liu, X., Tan, L., Wu, S., 2022. Two-dimensional antibacterial materials, Prog. Mater. Sci. 130, 100976.

Li, J., Wang, G., Zhu, H., Zhang, M., Zheng, X., Di, Z., 2015. Antibacterial activity of large-area monolayer graphene film manipulated by charge transfer. Sci. Rep. 4, 4359.

Lin, N., Berton, P., Moraes, C., Rogers, R.D., Tufenkji, N., 2018. Nanodarts, nanoblades, and nanospikes: Mechano-bactericidal nanostructures and where to find them. Adv. Colloid Interface Sci. 252, 55-68.

Linklater, D.P., Baulin, V.A., Juodkazis, S., Crawford, R.J., Stoodley, P., Ivanova, E.P. 2021. Mechano-bactericidal actions of nanostructured surfaces. Nat. Rev. Microbiol. 19, 8–22.

Linklater, D.P., Baulin, V.A., Juodkazis, S., Ivanova, E.P., 2018. Mechano-bactericidal mechanism of graphene nanomaterials. Interface Focus 8(3), 20170060.

Liu, B., Peng, S., Liao, Y., Long, W., 2018. The causes and impacts of water resources crises in the Pearl River Delta. J. Clean. Prod. 177, 413-425.

Liu, D., Zhou, W., Wu, J., Huang, T., 2018. Fractal characterization of graphene oxide nanosheets. Mater. Lett. 220, 40–43.

Liu, S., Wei, L., Hao, L., Fang, N., Chang, M.W., Xu, R., et al., 2009. Sharper and faster "Nano Darts" kill more bacteria: A study of antibacterial activity of individually dispersed pristine single-walled carbon nanotube. ACS Nano 3(12), 3891-3902.

Lu, C., Zeyu, L., Zongjin, L., Christopher, K.Y.L., 2016. Effect of graphene oxide on the mechanical behavior of strain hardening cementitious composites. Construct. Build. Mater. 120, 457–464.

Maksoud, M.A., El-Sayyad, G.S., El-Khawaga, A.M., Abd Elkodous, M., Abokhadra, A., Elsayed, M.A., 2020. Nanostructured Mg substituted Mn-Zn ferrites: A magnetic recyclable catalyst for outstanding photocatalytic and antimicrobial potentials. J. Hazard. Mater. 399, 123000.

Mann, R., Mitsidis, D., Xie, Z., McNeilly, O., Ng, Y.H., Amal, R., Gunawan, C., 2021. Antibacterial activity of reduced graphene oxide. J. Nanomater. 2021, 9941577.

Mohammed, H., Kumar, A., Bekyarova, E., Al-Hadeethi, Y., Zhang, X., Chen, M., et al., 2020. Antimicrobial mechanisms and effectiveness of graphene and graphene-functionalized biomaterials. A scope review, Front. Bioengin. Biotechnol. 8, 465.

Mokammel, M.A., Islam, M.J., Hasanuzzaman, M., Saleem, M., Hashmi, J., 2022. Nanoscale materials for self-cleaning and antibacterial applications, Editor(s): Abdul-Ghani Olabi, Encyclopedia of Smart Materials, Elsevier, 315-324.

Naseer, F., Zahir, E., Danish, E.Y., Gull, M., Noman, S., Soomro, M.T., 2020. Superior antibacterial activity of reduced graphene oxide upon decoration with iron oxide nanorods. J. Environ. Chem. Eng. 8, 104424.

Naskar, A., Khan, H., Sarkar, R., Kumar, S., Halder, D., Jana, S., 2018. Anti-biofilm activity and food packaging application of room temperature solution process based polyethylene glycol capped Ag-ZnO-graphene nanocomposite. Mat. Sci. Eng. C. 91, 743-753.

Omran, B., Baek, K-H., 2022. Graphene-derived antibacterial nanocomposites for water disinfection: Current and future perspectives, Environ. Pollut. 298, 118836.

Orou, S.F.C., Hang, K.J., Thien, M.T., Ying, Y. L., Foh, L.C., Diem, N.D.N., et al., 2018. Antibacterial activity by ZnO nanorods and ZnO nanodisks: A model used to illustrate “Nanotoxicity Threshold”. J. Indust. Engin. Chem. 62, 333-340.

Parwez, K., Budihal, S.V., 2019. Quality control and risk management of carbon nanomaterials, in

Perspective of Carbon Nanotubes. London, United Kingdom: IntechOpen.

Pham, V.T.H., Truong, V.K., Quinn, M.D.J., Notley, S.M., Guo, Y., Baulin, V.A., 2015. Graphene induces formation of pores that kill spherical and rod-shaped bacteria. ACS Nano 9, 8458–8467.

Pieper, H., Chercheja, S., Eigler, S., Halbig, C.E., Filipovic, M.R., Mokhir, A., 2016. Endoperoxides revealed as origin of the toxicity of graphene oxide. Angew. Chemie Inter. Ed. 55(1), 405-407.

Rajapaksha, P., Cheeseman, S., Hombsch, S., Murdoch, B.J., Gangadoo, S., Blanch, E.W., et al., 2019. Antibacterial properties of graphene oxide–copper oxide nanoparticle nanocomposites. ACS Appl. Bio Mater. 2 (12), 5687– 5696.

Ranjani, S., Matheen, A., Antony, J.A., Hemalatha, S., 2021. Nanotechnology derived natural poly bio-silver nanoparticles as a potential alternate biomaterial to protect against human pathogens. Mater. Lett. 304, 30555**.**

Safdar, M., Kim, W., Park, S., Gwon, Y., Kim, Y-O., Kim, J. 2022. Engineering plants with carbon nanotubes: a sustainable agriculture approach. J. Nanobiotechnol. 20, 275.

Samak, N.A., Selim, M.S., Hao, Z., Xing, J., 2020. Controlled-synthesis of alumina-graphene oxide nanocomposite coupled with DNA/sulfide fluorophore for eco-friendly “Turn off/on” H_2S nanobiosensor. Talanta 211, 120655.

Samak, N.A., Selim, M.S., Hao, Z., Xing, J., 2022. Immobilized arginine/tryptophan-rich cyclic dodecapeptide on reduced graphene oxide anchored with manganese dioxide for microbial biofilm eradication. J. Hazard. Mater. 426, 128035.

Selim, M.S., El-Safty, S.A., Fatthallah, N.A., Shenashen, M.A., 2018. Silicone/graphene oxide sheet-alumina nanorod ternary composite for superhydrophobic antifouling coating. Prog. Org. Coat. 121, 160-172.

Selim, M.S., Mo, P.J., Hao, Z., Fatthallah, N.A., Chen, X., 2020b. Blade-like structure of graphene oxide sheets decorated with cuprous oxide and silicon carbide nanocomposites as bactericidal materials. J. Colloid Interface Sci. 578, 698-709.

Selim, M.S., Samak, N.A., Hao, Z., Xing, J., 2020a. Facile design of reduced graphene oxide

decorated with Cu_2O nanocube composite as antibiofilm active material. Mater. Chem. Phys. 239, 122300.

Selim, M.S., Shenashen, M.A., El-Safty, S.A., Sakai, M., Higazy, S.A., Selim, M.M., et al., 2017. Recent progress in marine foul-release polymeric nanocomposite coatings. Prog. Mater. Sci. 87, 1-32.

Sengupta, I., Bhattacharya, P., Talukdar, M., Neogi, S., Pal, S.K., Chakraborty, S., 2019. Bactericidal effect of graphene oxide and reduced graphene oxide: Influence of shape of bacteria. Colloid Interface Sci. Commun. 28, 60-68.

Shabanzade, H., Salem, A., Salem, S., 2018. Management of adsorbent content in waste motor oil regeneration by spectrophotometrical study and effective acidification in production of nano-porous clay. Spectrochim. Acta A Mol. Biomol. Spectrosc. 202, 214-221.

Shulga, N.N., Shulga, I.S., 2019. Antibacterial properties of graphene-based nanomaterials. Nanomaterials (Basel) 9, 737;

Singh, S., Datta, S., Narayanan, K.B., Rajnish, K.N., 2021. Bacterial exo-polysaccharides in biofilms: role in antimicrobial resistance and treatments. J. Genet Eng. Biotechnol. 19, 140.

Teixeira-Santos, R., Gomes, M., Gomes, L.C., Mergulhão, F.J., 2021. Antimicrobial and anti-adhesive properties of carbon nanotube-based surfaces for medical applications: a systematic review. iScience 24 (1), 102001.

Thebo, K.H., Qian, X., Wei, Q., Zhang, Q., Cheng, H.M., Ren, W., 2018. Reduced graphene oxide/metal oxide nanoparticles composite membranes for highly efficient molecular separation. J. Mater. Sci. Technol. 34 (9), 1481-1486.

Varjani, S.J., Upasani, V.N., 2017. A new look on factors affecting microbial degradation of petroleum hydrocarbon pollutants. Inter. Biodeter. Biodegrad. 120, 71-83.

Wang, Z., Zhu, W., Qiu, Y., Yi, X., von dem Bussche, A., Kane, A., et al., 2016. Biological and environmental interactions of emerging two-dimensional nanomaterials. Chem. Soc. Rev. 45, 1750–1780.

Xia, M-Y., Xie, Y., Yu, C-H., Chen, G-Y., Li, Y-H., Zhang, T., 2019. Graphene-based nanomaterials: the promising active agents for antibiotics-independent antibacterial applications. J. Control Release 307, 16-31.

Xin, Q., Shah, H., Nawaz, A., Xie, W., Akram, M.Z., Batool, A., et al., 2019. Antibacterial carbon-based nanomaterials, in Special Issue: Advanced Materials Research at NCNST. Adv. Mater. 31 (45), 1804838.

Yayehrad, A.T., Wondie, G.B., Marew, T., 2022. Different nanotechnology approaches for *Ciprofloxacin* delivery against multidrug-resistant microbes. Infect. Drug Resist. 15, 413–426.

Yuan, X., Zhang, X., Sun, L., Wei, Y., Wei, X., 2019. Cellular toxicity and immunological effects of carbon-based nanomaterials. Part Fibre Toxicol. 16(1), 18.

Zhang, T., Tremblay, P-L., 2020. Graphene: An antibacterial agent or a promoter of bacterial proliferation, iScience 23 (12), 101787.

Zheng, Q., Han, B., Cui, X., Yu, X., Ou, J., 2017. Graphene-engineered cementitious composites: small makes a big impact. Nanomater. Nanotechnol. 7, 1-18.

List of Figures:

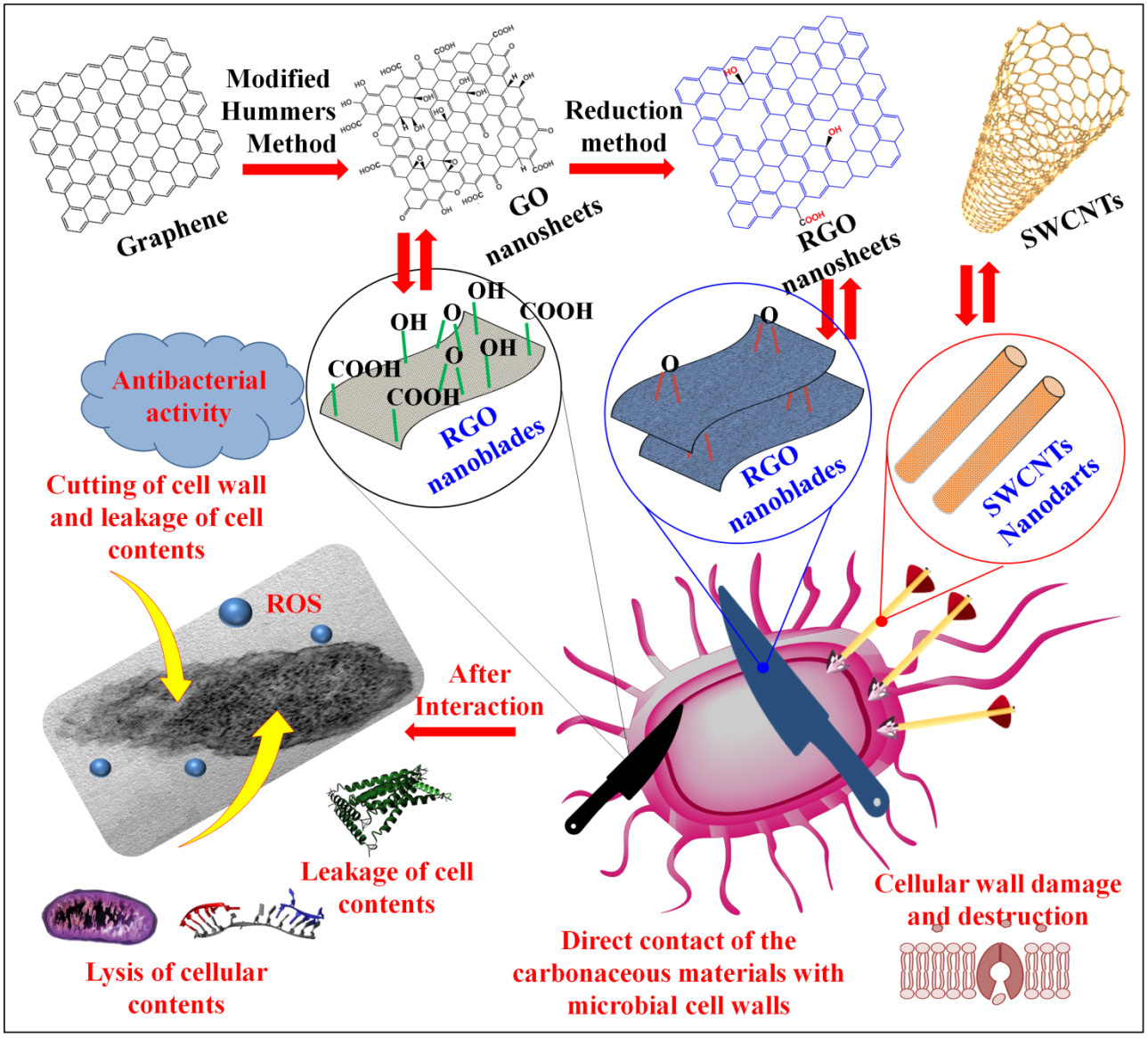
Graphene
Modified Hummers Method
GO nanosheets
Reduction method
RGO nanosheets
SWCNTs
Antibacterial activity
RGO nanoblades
SWCNTs Nanodarts
Cutting of cell wall and leakage of cell contents
ROS
After Interaction
Leakage of cell contents
Lysis of cellular contents
Direct contact of the carbonaceous materials with microbial cell walls
Cellular wall damage and destruction

Scheme 1.

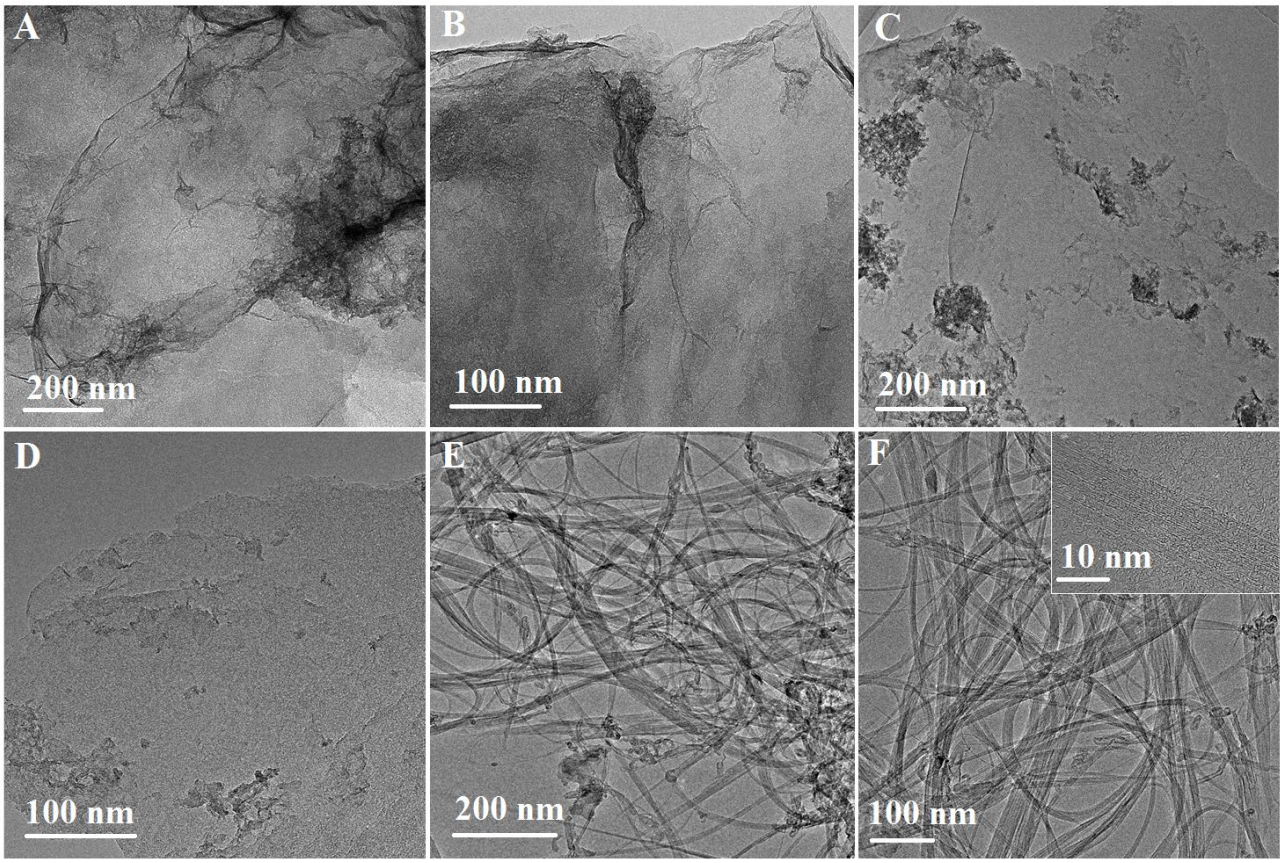

Fig. 1.

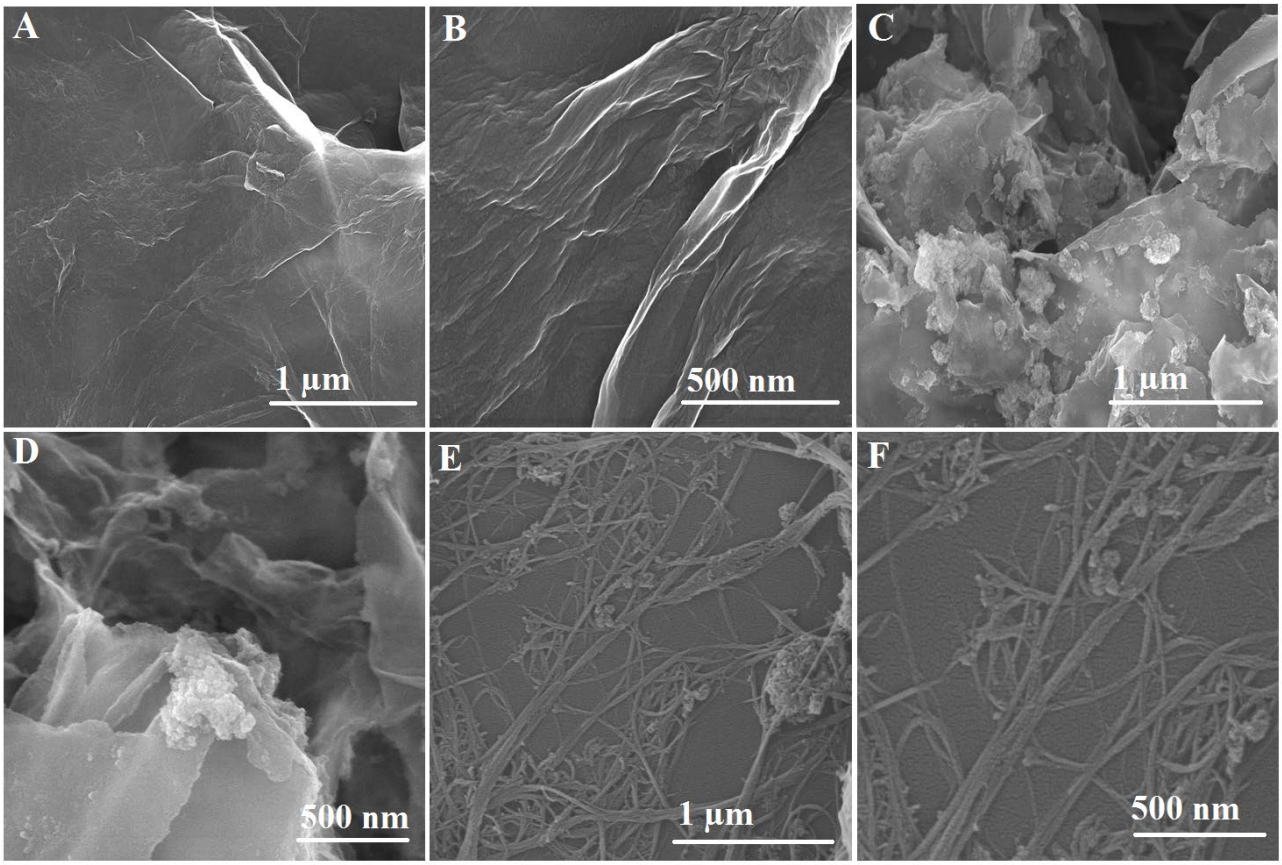

Fig. 2.

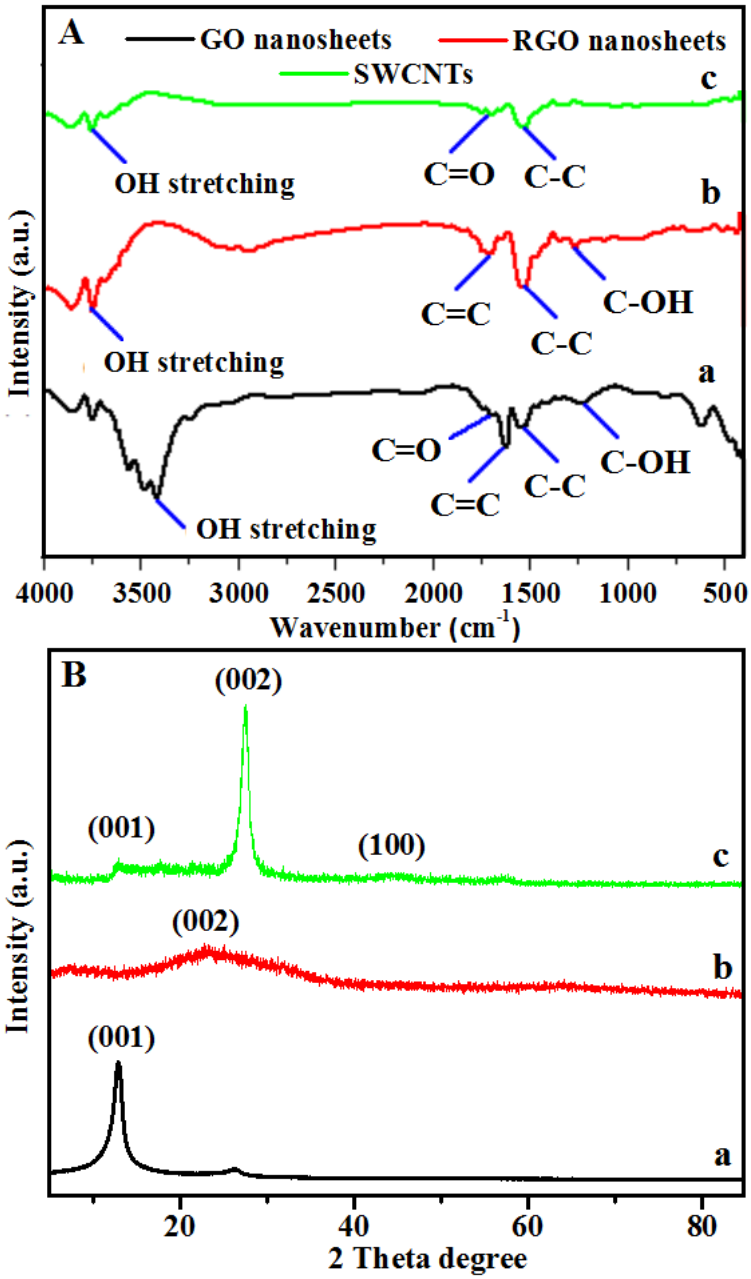
A
GO nanosheets
RGO nanosheets
SWCNTs
c
OH stretching
C=O
C-C
b
C=C
C-OH
C-C
OH stretching
a
C=O
C-OH
C-C
C=C
OH stretching
Intensity (a.u.)
4000
3500
3000
2500
2000
1500
1000
500
Wavenumber (cm-1)
B
(002)
(001)
(100)
c
(002)
b
(001)
a
Intensity (a.u.)
20
40
60
80
2 Theta degree

Fig. 3.

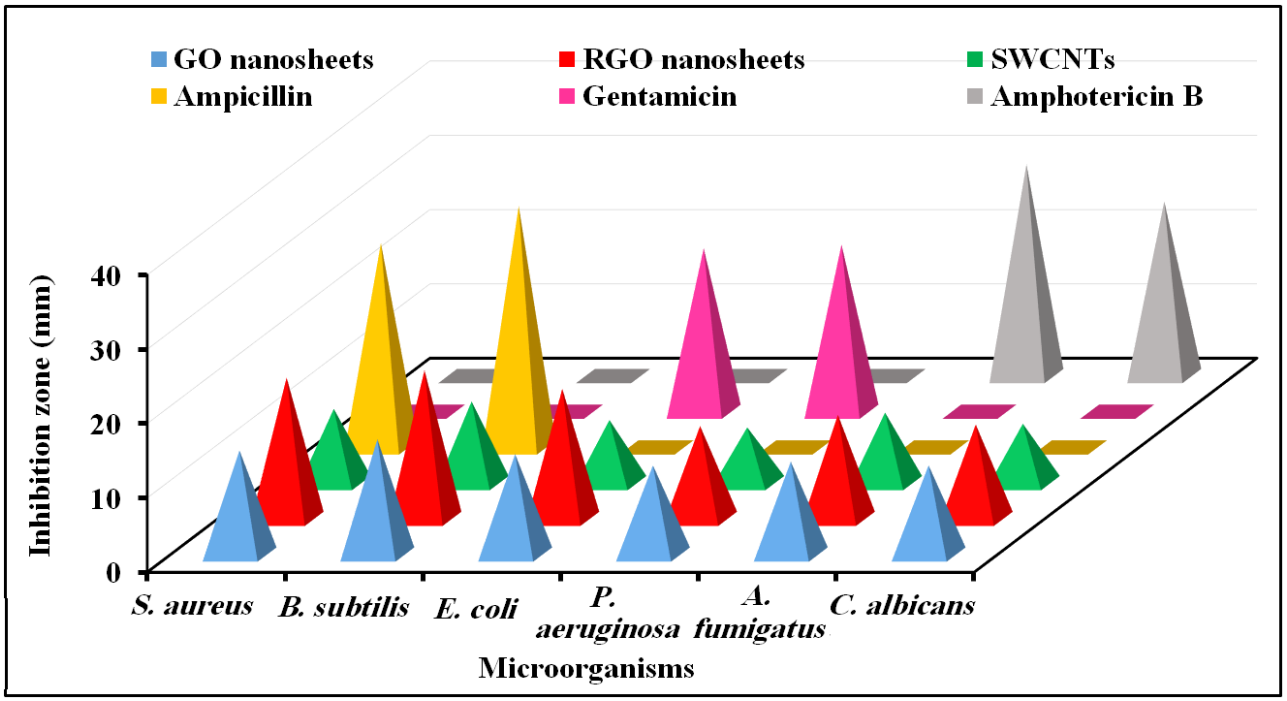
GO nanosheets
RGO nanosheets
SWCNTs
Ampicillin
Gentamicin
Amphotericin B
Inhibition zone (mm)
40
30
20
10
0
S. aureus
B. subtilis
E. coli
P. aeruginosa
A. fumigatus
C. albicans
Microorganisms

Fig. 4.

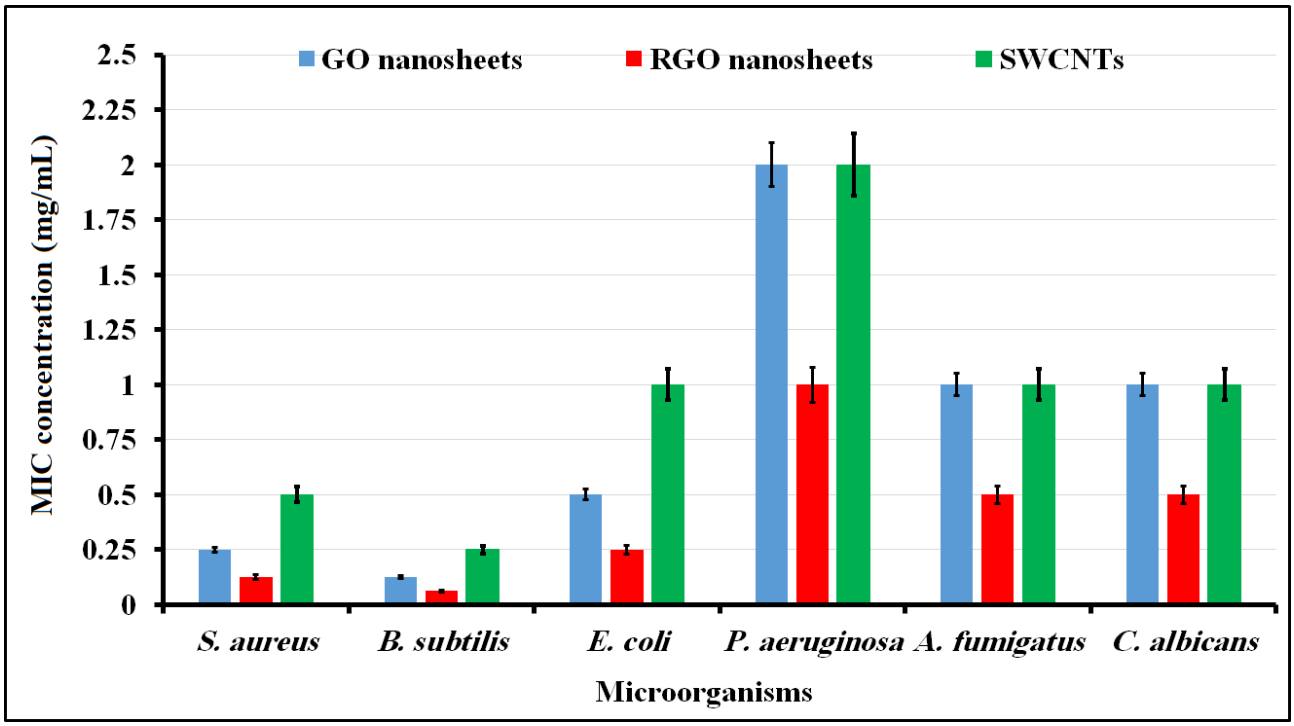
GO nanosheets
RGO nanosheets
SWCNTs
MIC concentration (mg/mL)
2.5
2.25
2
1.75
1.5
1.25
1
0.75
0.5
0.25
0
S. aureus
B. subtilis
E. coli
P. aeruginosa
A. fumigatus
C. albicans
Microorganisms

Fig. 5.

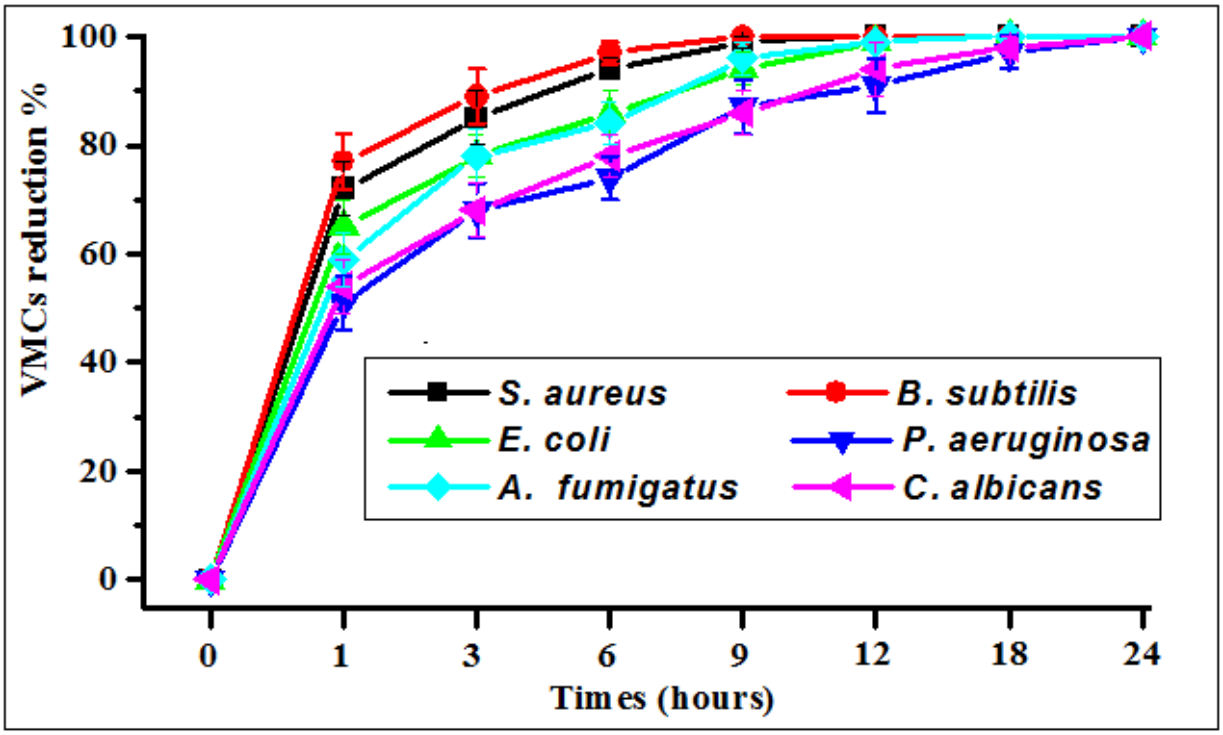
VMCs reduction %
100
80
60
40
20
0
0
1
3
6
9
12
18
24
Times (hours)
S. aureus
B. subtilis
E. coli
P. aeruginosa
A. fumigatus
C. albicans

Fig. 6.

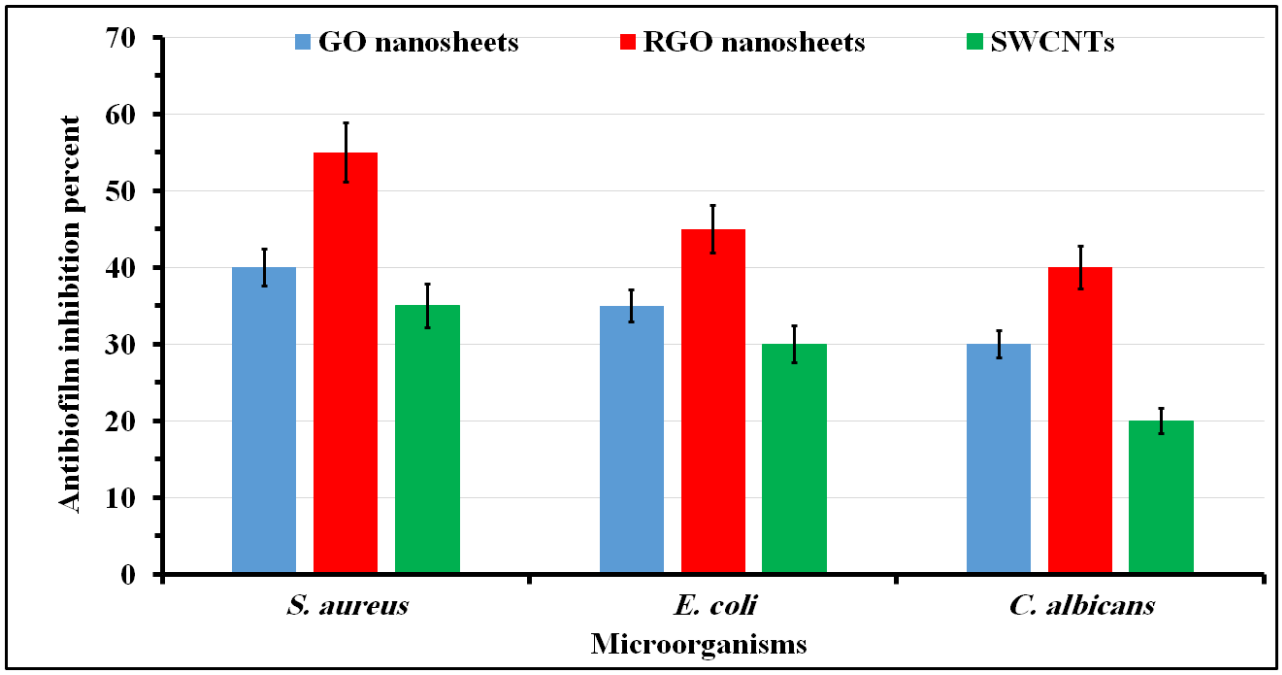
GO nanosheets
RGO nanosheets
SWCNTs
Antibiofilm inhibition percent
70
60
50
40
30
20
10
0
S. aureus
E. coli
C. albicans
Microorganisms

Fig. 7.

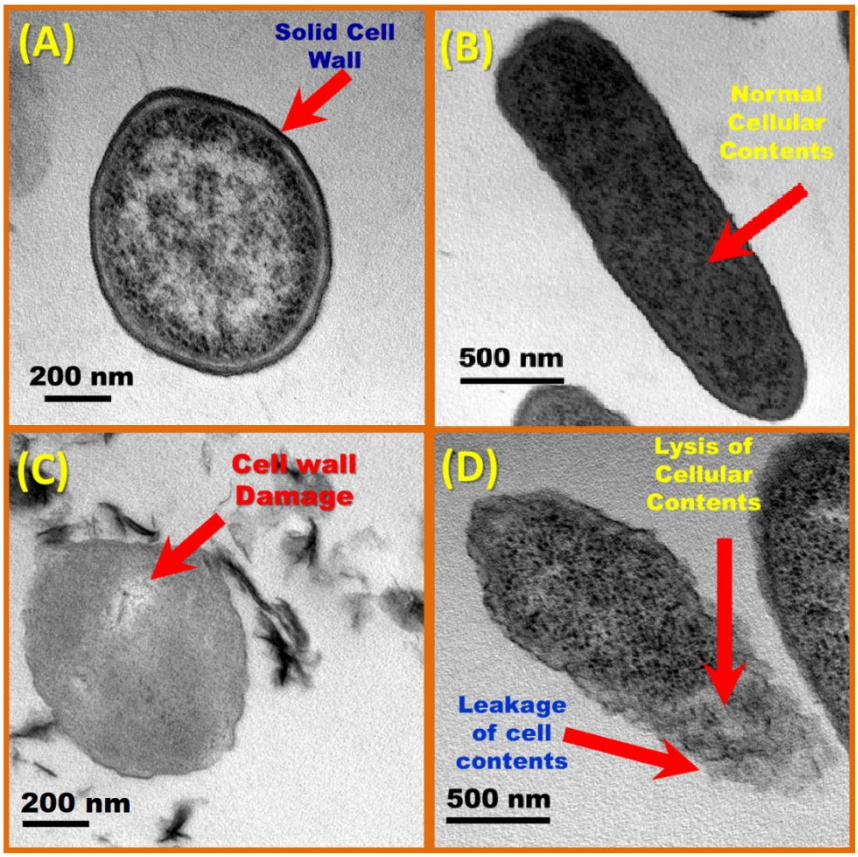
(A)
Solid Cell Wall
200 nm
(B)
Normal Cellular Contents
500 nm
(C)
Cell wall Damage
200 nm
(D)
Lysis of Cellular Contents
Leakage of cell contents
500 nm

Fig. 8.